Journal of Magnetic Resonance 200 (2009) 173–177

Contents lists available at ScienceDirect

Journal of Magnetic Resonance

journal homepage: www.elsevier.com/locate/jmr

Using multiple quantum coherence to increase the ^{15}N resolution in a three-dimensional TROSY HNCO experiment for accurate PRE and RDC measurements

Kaifeng Hu, Michaeleen Doucleff, G. Marius Clore *

Laboratory of Chemical Physics, National Institute of Diabetes and Digestive and Kidney Diseases, National Institutes of Health, Bethesda, MD 20892-0520, USA

ARTICLE INFO

Article history:
Received 31 March 2009
Revised 23 June 2009
Available online 27 June 2009

Keywords:
TROSY HNCO
High resolution
RDC
PRE

ABSTRACT

We present a new version of the 3D TROSY HNCO pulse scheme, referred to as HR-TROSY HNCO, with comparable resolution in the ^{15}N dimension to a 2D ^{1}H–^{15}N HSQC experiment. In the conventional 3D TROSY HNCO, the constant time period ($1/2J_{NC} \sim 32$ ms) severely limits the maximum resolution in the ^{15}N dimension. In the HR-TROSY HNCO experiment presented here, both constant time periods ($\sim$32 ms each) for coherence forward and backward transfer between ^{15}N and ^{13}C′ are utilized to double the ^{15}N evolution time. This leads to a dramatic enhancement in peak separation along the ^{15}N dimension, making the HR-TROSY HNCO an ideal pulse scheme for accurate paramagnetic relaxation enhancement and residual dipolar coupling measurements.

Published by Elsevier Inc.

1. Introduction

In recent years, several NMR methods, which complement traditional NOE-based approaches, have been developed to facilitate three-dimensional structure determination, to characterize molecular motions, and to visualize lowly-populated transient species. In particular, residual dipolar couplings (RDC) yield bond vector orientations relative to an external alignment tensor that are particularly useful for structure determination of multidomain proteins, protein complexes and nucleic acids [1–4]. In addition, accurate RDC data can potentially be used to study protein dynamics [5–13]. Paramagnetic relaxation enhancement (PRE) provides long-range distance information (up to $\sim$35 Å in suitable cases) that is particularly useful in the study of macromolecular complexes [14–16] and has been recently exploited to characterize highly transient, lowly-populated species [17–24], as well as unfolded and disordered states of proteins [25–27].

In cases where resolution permits, conventional backbone amide RDCs and PREs can be measured using 2D ^{1}H–^{15}N HSQC- or TROSY- [28] based experiments [29,20], allowing the rapid measurement of a large number of RDCs and PREs. However, for larger proteins, or moderately-sized proteins with high α helical or unstructured coil content, cross-peak overlap greatly decreases the accuracy of the measured peak splittings and intensities.

Yang et al. extended the 2D ^{1}H–^{15}N correlation experiment to a 3D TROSY-based HNCO to separate overlapped peaks along an additional ^{13}C′ dimension for the measurement of $^{1}D_{NH}$ RDCs [30]. In principle, a similar HNCO scheme can also be implemented for PRE Γ_2 measurements by simply replacing the first INEPT element by a PRE measuring block [20]. However, the conventional TROSY-based HNCO [31] suffers from extremely low resolution along the ^{15}N dimension because the maximum ^{15}N evolution time is limited by the constant time period ($1/2J_{NC'} \sim 32$ ms), for coherence back transfer from ^{13}C′ to ^{15}N, and resolution is inversely proportional to this evolution time. As a result, RDCs and PREs measured along the ^{15}N dimension in a conventional TROSY HNCO would result in lower precision compared to the 2D ^{1}H–^{15}N HSQC counterpart.

Here, we present a high-resolution version of the TROSY HNCO, which we refer to as HR-TROSY HNCO, in which both constant time periods ($\sim$32 ms each) for coherence forward and backward transfer between ^{15}N and ^{13}C′ are utilized to maximize the ^{15}N evolution period, thereby extending the ^{15}N evolution time of 64 ms. This experiment separates cross-peaks along the ^{13}C′ dimension while maintaining high resolution along the ^{15}N dimension. An HNCO pulse scheme with improved resolution along the ^{15}N dimension was previously proposed by Madsen and Sørensen [32]. In the latter implementation only the ^{15}N to ^{13}C′ (forward) INEPT transfer period ($\sim$32 ms) is utilized for ^{15}N chemical shift evolution, and improved resolution along the ^{15}N dimension is realized by varying the evolution period from -32 to 32 ms by shifting the 180° pulses from one end of the constant time period to the other. This concept can also be easily incorporated into our HR-TROSY HNCO pulse sequence which would further extend the evolution time from -64 to 64 ms. We demonstrate the utility of the 3D HR-TROSY HNCO

* Corresponding author. Fax: +1 301 496 0825.
E-mail address: mariusc@intra.niddk.nih.gov (G.M. Clore).

1090-7807/$ - see front matter Published by Elsevier Inc.
doi:10.1016/j.jmr.2009.06.019

experiment on a 1:1 complex of U-[^{15}N, ^{13}C, ^{2}H]-labeled mouse KIX with phosphorylated KID (pKID) [33].

2. Experimental

2.1. Materials

A 29 residue peptide (pKID) comprising the kinase-inducible domain of the cAMP response-element binding protein (CREB, residues 119–146) was synthesized by solid state methods with Ser133 phosphorylated, the N-terminus acetylated, and the C-terminus amidated (Biopeptide Co., San Diego). U-[^{15}N, ^{13}C, ^{2}H]-labeled mouse KIX domain (residues 586–672 of the CREB binding protein) was expressed and purified essentially as described previously [33].

2.2. NMR experiments

All NMR spectra were recorded at 27 °C on a Bruker 600 MHz spectrometer equipped with a *z*-gradient triple resonance cryoprobe. A 2D ^{1}H–^{15}N HSQC spectrum (non-constant time) was recorded as a reference with $128(t_1) \times 512(t_2)$ complex points along the ^{15}N and ^{1}H dimensions corresponding to acquisition times of 64 and 63.9 ms, respectively. The data matrix for the HR-TROSY HNCO comprises $100(t_1) \times 10(t_2) \times 512(t_3)$ complex points along the ^{15}N, ^{13}C′ and ^{1}H dimensions corresponding to acquisition times of 63.24, 8.28 and 77.4 ms, respectively. The HR-TROSY HNCO spectrum was recorded with 16 scans per increment and an interscan delay of 1.1 s, resulting in ~18 h of total measurement time. For comparison, a conventional TROSY HNCO was recorded with $50(t_1) \times 10(t_2) \times 512(t_3)$ complex points along the ^{15}N, ^{13}C′ and ^{1}H dimensions corresponding to acquisition times of 31.62, 8.28 and 77.4 ms, respectively, using 32 scans per increment, resulting in the same total measurement time as the HR-TROSY HNCO. For both the HR-TROSY HNCO and conventional TROSY experiments the ^{15}N, ^{13}C′ and ^{1}H carrier frequencies were placed at 117, 176 and 4.75 ppm, respectively, and the sweep widths in the corresponding dimensions were 26, 8 and 11.02 ppm, respectively. (The same carrier frequencies and sweep widths for ^{1}H and ^{15}N were also used for the ^{1}H–^{15}N HSQC.) The conventional TROSY and HR-TROSY HNCO spectra were processed identically using linear prediction and zero-filling along the ^{15}N dimension, giving final spectra with 256 and 512 frequency data points, respectively. Replacing the first INEPT element (dashed block in Fig. 1A) with the PRE measuring block (Fig. 1B) adapts the HR-TROSY HNCO pulse sequence to one suitable for PRE Γ_2 measurements. By setting the transverse relaxation delay T_1 to be 0 and 14 ms and acquiring the data for both delays in an interleaved manner [20], the total experimental time is ~39 h. All data sets were processed using the NMRPipe package [34].

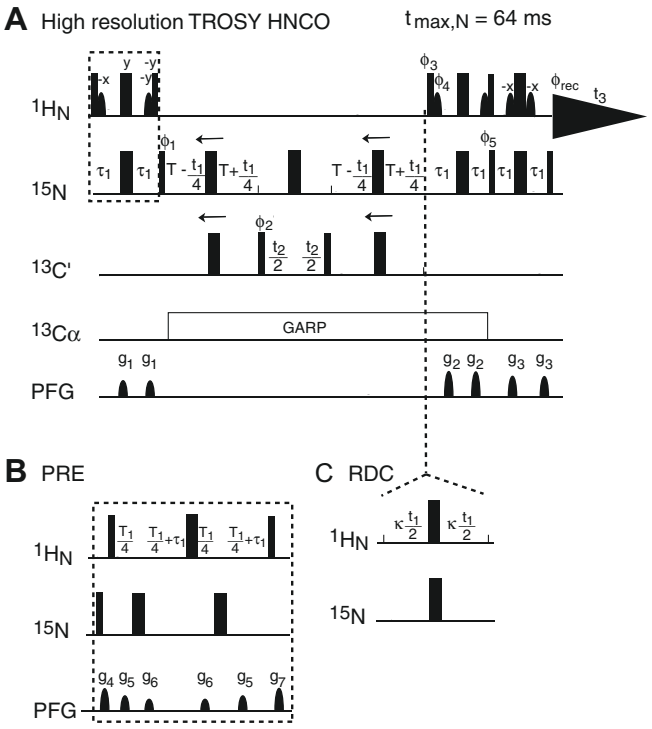

Fig. 1. (A) Pulse sequence of the 3D HR-TROSY HNCO with high resolution along the ^{15}N dimension. The radio-frequency pulses on ^{1}H, ^{15}N, ^{13}C′ and ^{13}C$^{\alpha}$ are applied at 4.75, 117, 176 and 56 ppm, respectively. Narrow and wide black bars indicate non-selective 90° and 180° pulses, respectively. Water suppression is achieved using the Watergate pulse train. ^{13}C$^{\alpha}$ decoupling is carried out using GARP with a field strength of $\gamma B_2 = 0.625$ kHz. Sine bell shape ^{1}H pulses are water selective 90° pulses. The duration and strength of the pulsed field gradients applied along the *z*-axis are as follows: g_1: 0.7 ms, 25 G/cm; g_2: 1.0 ms, 60 G/cm; g_3: 0.7 ms, 50 G/cm; g_4: 0.45 ms, 50 G/cm; g_5: 0.3 ms, 21 G/cm; g_6: 0.3 ms, 19 G/cm. The delays are $T = 16$ ms, $\tau_1 = 2.72$ ms. The phase cycling is as follows: $\phi_1 = y, -y, x, -x$; $\phi_2 = 4x, 4(-x)$; $\phi_3 = -y$; $\phi_4 = y$; $\phi_5 = -y$; $\phi_{rec} = y, -y, -x, x, -y, y, x, -x$. All other radio-frequency pulses are applied with phase x except as indicated. A phase-sensitive spectrum in the ^{15}N (t_1) dimension is obtained by recording a second FID for each t_1 value, with $\phi_1 = y, -y, -x, x$; $\phi_3 = y$; $\phi_4 = -y$; and $\phi_5 = y$. Quadrature detection in the ^{13}C′ (t_2) dimension is achieved using States-TPPI applied to the phase ϕ_2. The resolution can be further improved [32] by simultaneously shifting the ^{15}N and ^{13}C′ 180° pulses from one end of the constant time period $2T$ to the other for the coherence forward and backward transfer between ^{15}N and ^{13}C′; that is by simply replacing the two $T - t_1/4$ periods by $2T - t_1/4$ periods, and the two $T + t_1/4$ periods by $t_1/4$ periods, thereby extending the ^{15}N evolution period from −64 to 64 ms. (B) Modification of the 3D HR-TROSY HNCO pulse sequence for measurement of PRE Γ_2 rates [20]. The INEPT element (dashed block in (A)) is replaced by the PRE measuring block (B). A two-time point measurement with different values of the relaxation delay T_1 is carried out in an interleaved mode. (C) Modification of the 3D HR-TROSY HNCO pulse sequence for measurement of ^{1}H$_N$–^{15}N dipolar couplings along the ^{15}N dimension. In the first instance (not shown), the anti-TROSY component of ^{15}N is simply selected by swapping the phases of ϕ_3 and ϕ_4 in (A): i.e $\phi_3 = y$; $\phi_4 = -y$. In the second instance, a $(J + D)$ coupling scaling element κt_1 is inserted without changing anything else [35] as indicated by the dashed lines. Usually the value of the scaling factor κ can be set to 1.

3. Results and discussion

Fig. 1A provides a schematic of the 3D HR-TROSY HNCO pulse scheme. After the first INEPT, magnetization on ^{15}N is transferred to ^{13}C′ and MQ coherence between ^{15}N and ^{13}C′ is generated by the 90° ^{13}C′ pulse (ϕ_2). By synchronously shifting the 180° ^{15}N and ^{13}C′ pulses (as indicated by the arrows), the chemical shift of ^{15}N is encoded during both constant time periods for the coherence forward and backward transfer between ^{15}N and ^{13}C′, thereby extending the maximum ^{15}N evolution time to as long as $1/J_{NC'} \sim 64$ ms. This allows the resolution along the ^{15}N dimension of the 3D HR-TROSY experiment to be comparable to that of the 2D ^{1}H–^{15}N HSQC counterpart. A similar approach has been previously reported for the 3D HNCA TROSY used for sequence specific backbone assignments [31], in which the maximum ^{15}N evolution time was $1/({}^{1}J_{NC\alpha} + {}^{2}J_{NC\alpha(i-1)}) \sim 44$ ms. The 3D HR-TROSY HNCO offers even higher resolution along the ^{15}N dimension, which results in better separation of amide cross-peaks and yields clearer 2D planes and strips.

Fig. 2A shows the overall 2D ^{1}H–^{15}N HSQC spectrum for the KIX/pKID complex, and an expansion of the most crowded region is provided in Fig. 2B. ^{1}H$_N$–^{13}C′ planes of the HR-TROSY HNCO and conventional TROSY HNCO spectra are displayed in Figs. 2C and D, respectively, taken at the ^{15}N chemical shifts corresponding to the dashed lines *a*–*e* in Fig. 2B. A comparison of Figs. 2C and D clearly demonstrates that the HR-TROSY HNCO spectrum is cleaner

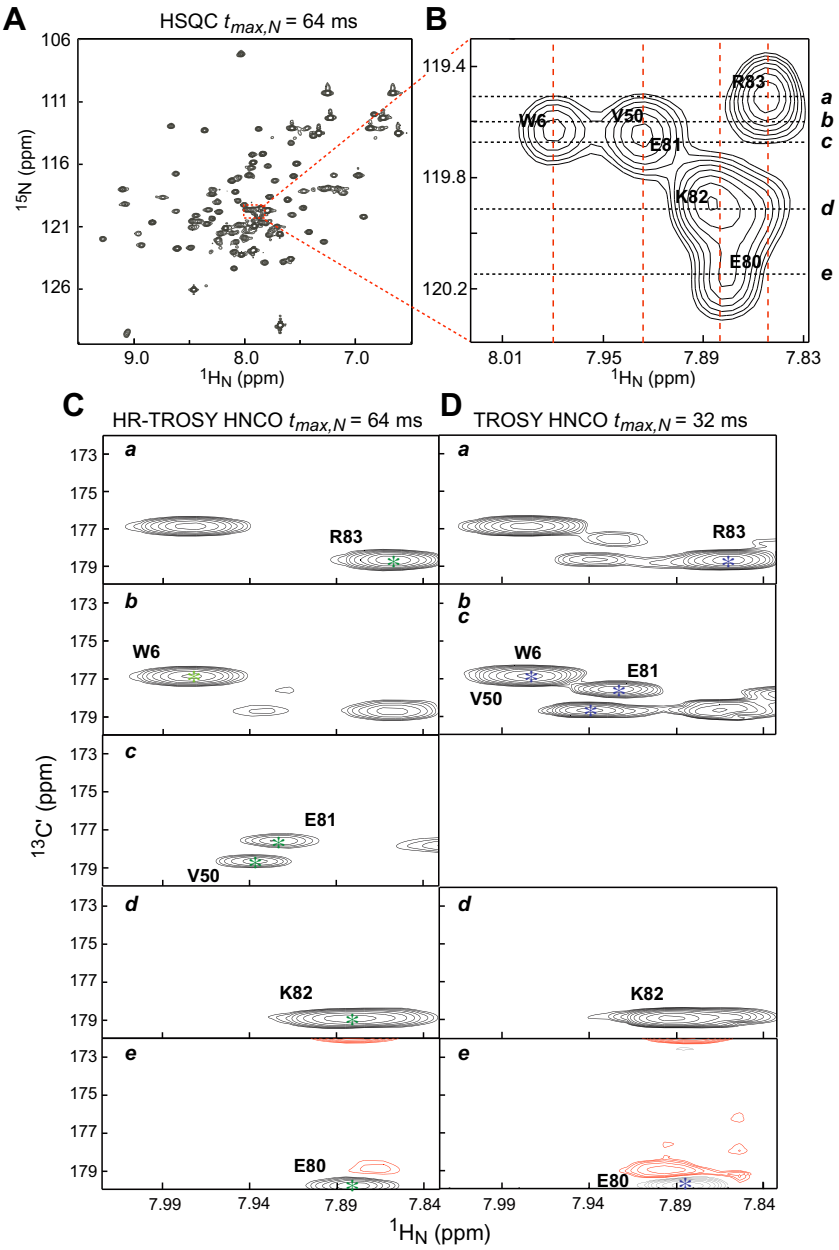

Fig. 2. Demonstration of increased ^{15}N resolution in the HR-TROSY HNCO spectrum. (A) 600 MHz 2D ^{1}H–^{15}N HSQC spectrum of 0.25 mM U-[^{15}N, ^{13}C, ^{2}H]-labeled mouse KIX complexed with pKID (1:1 stoichiometry) at 27 °C. (B) Expansion of a region with a high degree of spectral overlap to illustrate the high ^{15}N resolution afforded by the 3D HR-TROSY HNCO. Peaks assignments are annotated with the residue numbering for the KIX domain of CBP. (C), ^{1}H$_N$–^{13}C′ slices taken from the 3D HR-TROSY HNCO spectrum at the ^{15}N chemical shifts indicated by the dashed lines *a*–*e* in (B), showing a very clean spectrum with well-resolved cross-peaks. (D) The corresponding ^{1}H$_N$–^{13}C′ slices taken from the conventional 3D TROSY HNCO spectrum are shown for comparison. In the conventional TROSY HNCO, ^{1}H$_N$–^{13}C′ slices taken at the ^{15}N chemical shifts of dashed lines *b*–*c* are identical owing to complete overlap due to the low resolution along the ^{15}N dimension. In (C) and (D), peaks with red contours have negative signs arising from folding in the ^{13}C′ dimension. The red dashed lines in (B) and the green and blue stars in (C) and (D), respectively, indicate the positions where the 1D slices along the ^{15}N dimension shown in Fig. 3 were taken from the reference 2D ^{1}H–^{15}N HSQC, the 3D HR-TROSY HNCO and the conventional 3D TROSY HNCO, respectively.

and better resolved than the conventional TROSY HNCO, which exhibits significant peak leakage between different ^{1}H$_N$–^{13}C′ planes due to the lower ^{15}N resolution. Indeed, the ^{1}H$_N$–^{13}C′ planes taken from the conventional TROSY HNCO at the ^{15}N chemical shifts *b* and *c* are completely overlappped (identical). Fig. 3 provides a comparison of 1D traces along the ^{15}N dimension for the reference 2D ^{1}H–^{15}N HSQC (taken at the ^{1}H chemical shifts indicated by the red dashed lines in Fig. 2), the 3D HR-TROSY HNCO (taken at the cross-peak positions indicated by the green stars in Fig. 2C) and the conventional 3D TROSY HNCO (taken at the cross-peak positions indicated by the blue stars in Fig. 2D). These traces correspond to peaks for W6, V50, E80, E81, K82 and R83 (all peaks in the green traces have narrower linewidths than those in the blue traces). The increased resolution along the ^{15}N dimension makes the HR-TROSY HNCO particularly well suited for RDC and PRE measurements because peak positions and intensities can be measured more accurately in the 3D HR-TROSY HNCO than in the conventional 3D TROSY HNCO or 2D ^{1}H–^{15}N HSQC experiments.

During the constant time periods of the HR-TROSY HNCO, no decoupling or 180° pulse is applied on ^{1}H to maintain the ^{15}N coherence under the TROSY state. To minimize intensity attenuation on MQ coherence due to passive *J* couplings between ^{1}H and

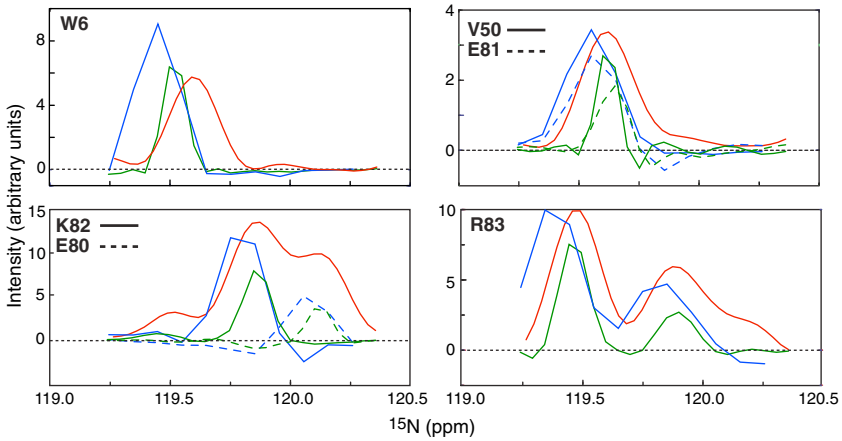

Fig. 3. 1D slices along the ^{15}N dimension from the 2D ^{1}H–^{15}N HSQC (red), the 3D HR-TROSY HNCO (green) and the conventional 3D TROSY HNCO (blue) for residues W6, V50, E80, E81, K82 and R83 of KIX in the U-[^{15}N,^{13}C,^{2}H]-KIX/pKID complex. Directly overlapping 1D ^{15}N peak profiles for these residues clearly illustrate the high resolution along the ^{15}N dimension afforded by the HR-TROSY HNCO (all peaks in green have narrower peak widths). The peak heights and noise levels from the different spectra are not normalized.

^{15}N (e.g., $^{2}J_{H\alpha N}$ and $^{3}J_{H\alpha(i-1)N}$) during the long ^{15}N evolution period (64 ms) and between ^{1}H and ^{13}C′ (e.g., $^{2}J_{H\alpha C'}$ and $^{3}J_{H\beta C'}$) during the ^{13}C′ evolution period (t_2), we recommend perdeuterated samples for this type of experiment even for proteins of moderate molecular size. This is especially important when measuring peak intensities. Clear recognition of resolved cross-peaks with nearly undistorted peak shape is critical for measuring both peak position and intensity, which are important for accurate measurement of $^{1}D_{NH}$ RDCs and $^{1}H_N$ PRE relaxation rates, respectively.

Indeed, this basic 3D HR-TROSY HNCO pulse scheme is easily adapted to pulse sequences for the measurement of $^{1}H_N$–^{15}N PRE Γ_2 rates [20] (Fig. 1B) and $^{1}D_{NH}$ RDCs (Fig. 1C). For PRE measurements, the INEPT element (delineated by the dashed block in Fig. 1A) is replaced by the PRE measuring block (Fig. 1B). For RDC measurements, two alternative schemes are available. For proteins of moderate molecular size, where the anti-TROSY component of ^{15}N is not extremely broad and the peak shape remains undistorted, the anti-TROSY component can be directly selected by simply swapping the phases of ϕ_3 and ϕ_4 in the pulse scheme shown in Fig. 1A; selection of the TROSY and anti-TROSY components of ^{15}N can be run in an interleaved mode to obtain a pair of peaks, from which the splitting J or $(J + D)$ is measured. When the relaxation of the anti-TROSY component of ^{15}N is too fast or the peak shape is severely distorted, a $(J + D)$ coupling scaling element κt_1 is inserted [35] as indicated by the dashed lines in Fig. 1, and no other changes are necessary. In this case, the relevant coherence is under the TROSY state during the two constant time periods (total as long as 64 ms), which better optimizes the relaxation properties of the pulse scheme. Insertion of the κt_1 element allows the relevant coherence to evolve under the Hamiltonian $(J + D)$. The measured splitting between the peak of this scheme and that of the original HR-TROSY HNCO along the ^{15}N dimension is $(J + D)$ scaled by a factor of $\kappa/2$. In most cases, the optimal value of the scaling factor κ is 1. Lerche et al. [36] previously suggested a scheme for measuring $^{1}D_{NH}$ RDCs along the $^{1}H_N$ dimension in which the anti-TROSY and TROSY components of $^{1}H_N$ or the neutral (decoupled or refocused) $^{1}H_N$ chemical shift are chosen for the measurement of the couplings (J or $J + D$). To avoid potential linewidth broadening along the $^{1}H_N$ dimension due to passive ^{1}H–^{1}H RDCs, we made use of an ST2-PT element [37] in our pulse sequence to select the TROSY or anti-TROSY component for measuring $^{1}D_{NH}$ RDCs along the ^{15}N dimension while detecting $^{1}H_N$ under the TROSY state.

Acknowledgments

This work was supported by the intramural program of NIDDK, National Institutes of Health, and the Intramural AIDS Targeted Antiviral Program of the Office of the Director of the National Institutes of Health (to G.M.C.).

References

[1] N. Tjandra, A. Bax, Direct measurement of distances and angles in biomolecules by NMR in a dilute liquid crystalline medium, Science 278 (1997) 1111–1114.
[2] G.M. Clore, Accurate and rapid docking of protein–protein complexes on the basis of intermolecular nuclear overhauser enhancement data and dipolar couplings by rigid body minimization, Proc. Natl. Acad. Sci. USA 97 (2000) 9021–9025.
[3] J.H. Prestegard, H.M. al-Hashimi, J.R. Tolman, NMR structures of biomolecules using field oriented media and residual dipolar couplings, Q. Rev. Biophys. 33 (2000) 371–424.
[4] A. Bax, G. Kontaxis, N. Tjandra, Dipolar couplings in macromolecular structure determination, Methods Enzymol. 339 (2001) 127–174.
[5] J.R. Tolman, Dipolar couplings as a probe of molecular dynamics and structure in solution, Curr. Opin. Struct. Biol. 11 (2001) 532–539.
[6] J.R. Tolman, H.M. Al-Hashimi, L.E. Kay, J.H. Prestegard, Structural and dynamic analysis of residual dipolar coupling data for proteins, J. Am. Chem. Soc. 123 (2001) 1416–1424.
[7] K.B. Briggman, J.R. Tolman, De novo determination of bond orientations and order parameters from residual dipolar couplings with high accuracy, J. Am. Chem. Soc. 125 (2003) 10164–10165.
[8] G.M. Clore, C.D. Schwieters, Amplitudes of protein backbone dynamics and correlated motions in a small α/β protein: correspondence of dipolar coupling and heteronuclear relaxation measurements, Biochemistry 43 (2004) 10678–10691.
[9] G.M. Clore, C.D. Schwieters, How much backbone motion in ubiquitin is required to account for dipolar coupling data measured in multiple alignment media as assessed by independent cross-validation?, J Am. Chem. Soc. 126 (2004) 2923–2938.
[10] G. Bouvignies, P. Bernado, S. Meier, K. Cho, S. Grzesiek, R. Bruschweiler, M. Blackledge, Identification of slow correlated motions in proteins using residual dipolar and hydrogen-bond scalar couplings, Proc. Natl. Acad. Sci. USA 102 (2005) 13885–13890.
[11] G.M. Clore, C.D. Schwieters, Concordance of residual dipolar couplings, backbone order parameters and crystallographic B-factors for a small α/β protein: a unified picture of high probability, fast atomic motions in proteins, J. Mol. Biol. 355 (2006) 879–886.
[12] O.F. Lange, N.A. Lakomek, C. Fares, G.F. Schroder, K.F. Walter, S. Becker, J. Meiler, H. Grubmuller, C. Griesinger, B.L. de Groot, Recognition dynamics up to microseconds revealed from an RDC-derived ubiquitin ensemble in solution, Science 320 (2008) 1471–1475.

[13] B. Vogeli, L.S. Yao, A. Bax, Protein backbone motions viewed by intraresidue and sequential H–N–H-alpha residual dipolar couplings, J. Biomol. NMR 41 (2008) 17–28.
[14] J.L. Battiste, G. Wagner, Utilization of site-directed spin labeling and high-resolution heteronuclear nuclear magnetic resonance for global fold determination of large proteins with limited nuclear overhauser effect data, Biochemistry 39 (2000) 5355–5365.
[15] J.D. Gross, N.J. Moerke, T. von der Haar, A.A. Lugovskoy, A.B. Sachs, J.E. McCarthy, G. Wagner, Ribosome loading onto the mRNA cap is driven by conformational coupling between eIF4G and eIF4E. Cell 115 (2003) 739–750.
[16] J. Iwahara, C.D. Schwieters, G.M. Clore, Ensemble approach for NMR structure refinement against ^{1}H paramagnetic relaxation enhancement data arising from a flexible paramagnetic group attached to a macromolecule, J. Am. Chem. Soc. 126 (2004) 5879–5896.
[17] J. Iwahara, G.M. Clore, Detecting transient intermediates in macromolecular binding by paramagnetic NMR, Nature 440 (2006) 1227–1230.
[18] C. Tang, J. Iwahara, G.M. Clore, Visualization of transient encounter complexes in protein–protein association, Nature 444 (2006) 383–386.
[19] A.N. Volkov, J.A. Worrall, E. Holtzmann, M. Ubbink, Solution structure and dynamics of the complex between cytochrome c and cytochrome c peroxidase determined by paramagnetic NMR, Proc. Natl. Acad. Sci. USA 103 (2006) 18945–18950.
[20] J. Iwahara, C. Tang, G.M. Clore, Practical aspects of ^{1}H transverse paramagnetic relaxation enhancement measurements on macromolecules, J. Magn. Reson. 184 (2007) 185–195.
[21] C. Tang, C.D. Schwieters, G.M. Clore, Open-to-closed transition in apo maltose-binding protein observed by paramagnetic NMR, Nature 449 (2007) 1078–1082.
[22] G.M. Clore, Visualizing lowly-populated regions of the free energy landscape of macromolecular complexes by paramagnetic relaxation enhancement, Mol. Biosyst. 4 (2008) 1058–1069.
[23] C. Tang, J.M. Louis, A. Aniana, J.Y. Suh, G.M. Clore, Visualizing transient events in amino-terminal autoprocessing of HIV-1 protease, Nature 455 (2008) 693–696.
[24] X. Xu, W. Reinle, F. Hannemann, P.V. Konarev, D.I. Svergun, R. Bernhardt, M. Ubbink, Dynamics in a pure encounter complex of two proteins studied by solution scattering and paramagnetic NMR spectroscopy, J. Am. Chem. Soc. 130 (2008) 6395–6403.
[25] C.W. Bertoncini, Y.S. Jung, C.O. Fernandez, W. Hoyer, C. Griesinger, T.M. Jovin, M. Zweckstetter, Release of long-range tertiary interactions potentiates aggregation of natively unstructured α-synuclein, Proc. Natl. Acad. Sci. USA 102 (2005) 1430–1435.
[26] M.M. Dedmon, K. Lindorff-Larsen, J. Christodoulou, M. Vendruscolo, C.M. Dobson, Mapping long-range interactions in α-synuclein using spin-label NMR and ensemble molecular dynamics simulations, J. Am. Chem. Soc. 127 (2005) 476–477.
[27] D.J. Felitsky, M.A. Lietzow, H.J. Dyson, P.E. Wright, Modeling transient collapsed states of an unfolded protein to provide insights into early folding events, Proc. Natl. Acad. Sci. USA 105 (2008) 6278–6283.
[28] K. Pervushin, R. Riek, G. Wider, K. Wuthrich, Attenuated T_2 relaxation by mutual cancellation of dipole–dipole coupling and chemical shift anisotropy indicates an avenue to NMR structures of very large biological macromolecules in solution, Proc. Natl. Acad. Sci. USA 94 (1997) 12366–12371.
[29] M. Ottiger, F. Delaglio, A. Bax, Measurement of *J* and dipolar couplings from simplified two-dimensional NMR spectra, J. Magn. Reson. 131 (1998) 373–378.
[30] D.W. Yang, R.A. Venters, G.A. Mueller, W.Y. Choy, L.E. Kay, TROSY-based HNCO pulse sequences for the measurement of ^{1}HN–^{15}N, ^{15}N–^{13}CO, ^{1}HN–^{13}CO, ^{13}CO–^{13}Cα and ^{1}HN–^{13}Cα dipolar couplings in ^{15}N, ^{13}C, ^{2}H-labeled proteins, J. Biomol. NMR 14 (1999) 333–343.
[31] M. Salzmann, K. Pervushin, G. Wider, H. Senn, K. Wuthrich, TROSY in triple-resonance experiments: New perspectives for sequential NMR assignment of large proteins, Proc. Natl. Acad. Sci. USA 95 (1998) 13585–13590.
[32] J.C. Madsen, O.W. Sørensen, Multidimensional NMR experiments with improved resolution, J. Magn. Reson. 100 (1992) 431–436.
[33] K. Sugase, H.J. Dyson, P.E. Wright, Mechanism of coupled folding and binding of an intrinsically disordered protein, Nature 447 (2007) 1021–1025.
[34] F. Delaglio, S. Grzesiek, G.W. Vuister, G. Zhu, J. Pfeifer, A. Bax, Nmrpipe – a multidimensional spectral processing system based on unix pipes, J. Biomol. NMR 6 (1995) 277–293.
[35] A. Rexroth, P. Schmidt, S. Szalma, T. Geppert, H. Schwalbe, C. Griesinger, New principle for the determination of coupling-constants that largely suppresses differential relaxation effects, J. Am. Chem. Soc. 117 (1995) 10389–10390.
[36] M.H. Lerche, A. Meissner, F.M. Poulsen, O.W. Sørensen, Pulse sequences for measurement of one-bond ^{15}N–^{1}H coupling constants in the protein backbone, J. Magn. Reson. 140 (1999) 259–263.
[37] K.V. Peruvshin, G. Wider, K. Wüthrich, Single transition-to-single transition polarization transfer (ST2-PT) in [^{15}N, ^{1}H]-TROSY, J. Biomol. NMR 12 (1998) 345–348.